Highly permeable polymeric membranes based on the incorporation of the functional water channel protein Aquaporin Z

Manish Kumar*, Mariusz Grzelakowski†, Julie Zilles*, Mark Clark*, and Wolfgang Meier†‡

*Department of Civil and Environmental Engineering, University of Illinois at Urbana–Champaign, 205 North Mathews Avenue, Urbana, IL 61801; and †Department of Chemistry, University of Basel, Klingelbergstrasse 80, CH-4056 Basel, Switzerland

The permeability and solute transport characteristics of amphiphilic triblock-polymer vesicles containing the bacterial water-channel protein Aquaporin Z (AqpZ) were investigated. The vesicles were made of a block copolymer with symmetric poly-(2-methyloxazoline)-poly-(dimethylsiloxane)-poly-(2-methyloxazoline) ($PMOXA_{15}$-$PDMS_{110}$-$PMOXA_{15}$) repeat units. Light-scattering measurements on pure polymer vesicles subject to an outwardly directed salt gradient in a stopped-flow apparatus indicated that the polymer vesicles were highly impermeable. However, a large enhancement in water productivity (permeability per unit driving force) of up to ≈800 times that of pure polymer was observed when AqpZ was incorporated. The activation energy (E_a) of water transport for the protein-polymer vesicles (3.4 kcal/mol) corresponded to that reported for water-channel-mediated water transport in lipid membranes. The solute reflection coefficients of glucose, glycerol, salt, and urea were also calculated, and indicated that these solutes are completely rejected. The productivity of AqpZ-incorporated polymer membranes was at least an order of magnitude larger than values for existing salt-rejecting polymeric membranes. The approach followed here may lead to more productive and sustainable water treatment membranes, whereas the variable levels of permeability obtained with different concentrations of AqpZ may provide a key property for drug delivery applications.

permeability | triblock copolymer | water treatment

Biological membranes have excellent water transport characteristics, with certain membranes able to regulate permeability over a wide range. The permeability of membranes such as those present in the proximal tubules of the human kidney (1) can be increased by insertion of specific water-channel membrane proteins known as Aquaporins (AQPs). Other biological membranes, such as those in mammalian optic lenses (2), erythrocytes (3), and many other cell membranes (4) are constitutively AQP-rich. The permeabilities of AQP-rich membranes are orders of magnitude higher than those observed for unmodified phospholipid membranes (5). Additionally, some members of the AQP family have excellent solute retention capabilities for small solutes such as urea, glycerol, and glucose, even at high water transport rates (5, 6). These properties result from the unique structure of the water-selective AQPs. These AQPs have six membrane-spanning domains and a unique hourglass structure (7) with conserved charged residues that form a pore that allows both selective water transport and solute rejection. The AQP used in this study was a bacterial aquaporin from *Escherichia coli*, Aquaporin Z (AqpZ). AqpZ was selected because it can enhance the permeability of lipid vesicles by an order of magnitude while retaining small uncharged solutes (5). Additionally, AqpZ can be expressed in relatively large quantities in *E. coli* and has been reported to be quite stable under different reducing conditions and at temperatures of 4°C (5)—properties that make it attractive for drug delivery and water treatment applications.

The AQP's high permeability and high specificity could be valuable for a variety of applications. High permeabilities and excellent solute retention of small solutes are important for water treatment in critical medical applications such as dialysis (8, 9) because they could lead to reduced equipment size and more efficient energy use. A significant improvement in the permeability of solute-rejecting membranes would also be a large step in improving the economics of desalination for drinking water applications. Desalination is becoming increasingly important for water production in semiarid coastal regions (10, 11). Reverse-osmosis membranes are most commonly used for this application, whereas the use of membranes in a forward-osmosis scheme is becoming more interesting to water planners (10, 12). Both of these processes need extensive pretreatment of the source water to remove particulates and microbial contaminants, but they provide excellent treatment for properly pretreated water. However, reverse osmosis requires large energy consumption, and forward osmosis will require large membrane areas. This is because of the low productivity of currently used commercial reverse-osmosis and forward-osmosis membranes. The AQP-rich membrane proposed here, when suitably supported, could be used in similar processes with lower energy or membrane area requirements. Finally, the ability to produce membranes with low initial permeabilities is desirable for drug delivery applications (13), whereas a high level of control over permeability could be an additional advantage in designing alternative delivery methods (14).

The effects of AQPs on the permeability of liposomes (5), frog oocytes (3), and cellular secretory vesicles have been studied (15). However, the low stability of biological membranes or synthesized lipid membranes for water treatment and drug delivery applications is an important disadvantage (16). Obtaining and processing large volumes of such membranes would also present technical challenges.

The use of synthetic polymers, in particular, lipid-bilayer-like amphiphilic block copolymers, is intriguing because they are chemically and mechanically stable while still providing an amphiphilic structure that allows incorporation of membrane proteins such as AQPs (17). Some membrane proteins have been functionally inserted into block copolymer membranes (18–21). These include the β-barrel *ompF* protein, the bacterial receptor *lamB* protein, and bacteriorhodopsin. Directed insertion of the eye lens AQP (Aquaporin 0) into similar block copolymer membranes has also been demonstrated (22), although this
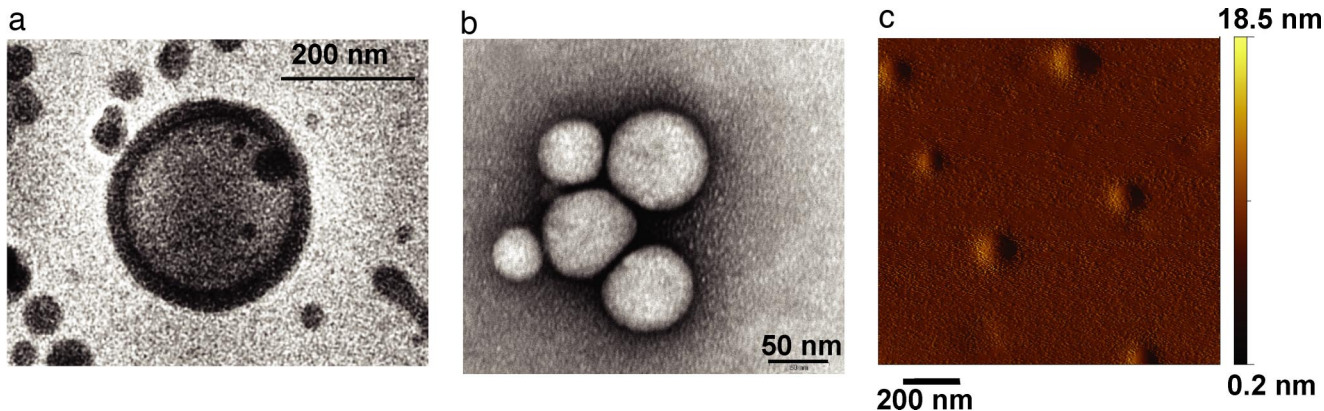
Fig. 1. Examination of polymer vesicles by using microscopy. The cryogenic transmission electron microscope images were used for size determination because regular transmission electron microscopy and atomic force microscopy influence the structure of the observed vesicles. (*a*) Cryogenic transmission electron micrograph of an ABA polymer vesicle. (Scale bar: 200 nm.) (*b*) Electron micrograph of a cluster of vesicles. (Scale bar: 50 nm.) (*c*) Atomic force micrograph of vesicles on mica in nontapping mode shows that a film of polymer is formed on the hydrophilic mica surface with vesicles located in the film. (Scale bar: 200 nm.)

initial study did not examine function. Additionally, there are few studies on the permeability of block copolymer membranes (13, 23), and no previous studies have reported on the magnitude of permeability improvement obtained by insertion of AQPs in block copolymer membranes. Data on rejection of dissolved ionic solutes such as salt (NaCl) have also not been reported for AQP-rich membranes.

To investigate the potential of protein-polymer membranes for the applications described above, solute and water transport properties and physical characteristics were analyzed for a specific protein-polymer membrane. This membrane was composed of a triblock copolymer with inserted AqpZ and is referred to throughout the text as an AqpZ-ABA membrane. The composition of the symmetric triblock copolymer was poly(2-methyloxazoline)-block-poly(dimethylsiloxane)-block-poly(2-methyloxazoline) ($PMOXA_{15}$-$PDMS_{110}$-$PMOXA_{15}$). This ABA polymer has a larger hydrophobic block (110 dimethylsiloxane units)-to-hydrophilic block (15 methyloxazoline units) ratio than those tested in previous studies (18, 19, 24–27). The physical characteristics of the ABA triblock copolymer were studied by using microscopy techniques, whereas light scattering was used to characterize the permeability.

Results

Synthesis of AqpZ-ABA Polymer Membranes. AqpZ was produced by a recombinant strain of *E. coli* by using a plasmid that allowed high levels of expression and incorporated 10 histidine residues at one end of the expressed protein to facilitate purification. This recombinant AqpZ was purified by using nickel affinity chromatography (5, 28). A large yield of pure protein (between 2.5 and 15 mg/liter of culture) was obtained for three different purification runs, indicating the potential for large yields by using the procedures described. $PMOXA_m$-$PDMS_n$-$PMOXA_m$ (ABA) triblock copolymers were synthesized by using a ring-opening cationic polymerization procedure. Polymer vesicles were produced by using the film rehydration method described in detail in *Materials and Methods*.

Characterization of Polymer Vesicles. To determine the permeability and solute rejection properties of polymer vesicles by using stopped-flow spectroscopy, a knowledge of the physical dimensions (radius in hydrated state) and morphology (hollow vs. solid sphere structure) is necessary. ABA polymer vesicles were therefore characterized by using static and dynamic light scattering, transmission electron microscopy, cryogenic transmission electron microscopy, and atomic force microscopy.

A hydrodynamic radius (R_h) of ≈160 nm was estimated from dynamic light scattering. This size is consistent with similar PMOXA-PDMS-based block copolymers with different hydrophilic-to-hydrophobic block length ratios (26). Dividing the radius of gyration (R_g) from static light-scattering experiments by the hydrodynamic radius from dynamic light scattering yields a value close to one ($R_g/R_h = 1.03$); this result is consistent with a hollow-sphere morphology (26). Static light scattering indicated a vesicle molecular weight of 52×10^6 g/mol.

The transmission electron microscope images indicate that the different vesicles have relatively uniform sizes. Cryogenic transmission electron microscopy indicated a hydrated vesicle radius of 117 nm. Fig. 1 shows representative images obtained from electron microscopy. Radii estimated from cryogenic transmission electron microscopy were used in further calculations of permeability as the rapid freeze used in this technique best preserves the hydrated vesicle's structural features (29).

The presence of spherical vesicle-like aggregates with a hydrophilic corona was further supported by atomic force microscopy measurements. When a dilute suspension of vesicles was spread on a hydrophilic mica surface, a film, punctuated with emerging vesicles, was observed (Fig. 1).

Permeability Measurements. The permeabilities of ABA and AqpZ-ABA vesicles were investigated by using stopped-flow light-scattering experiments as described in Borgnia *et al.* (5). Vesicle suspensions were rapidly mixed with osmotic solutions (1.7 osmol/liter) of salt (NaCl). The shrinkage of these vesicles was followed by monitoring the increase in light scattering over time. The initial rise in the experimental data was fitted to an exponential rise equation, and the exponential coefficient (k) was used to calculate permeability. These results are shown in Fig. 2 for the ABA and AqpZ-ABA vesicles with a protein-to-polymer molar ratio of 1:200. The time scale of initial rise for AqpZ-ABA vesicles was between 5 and 20 ms, whereas the lower permeability of the ABA vesicles led to a much longer rise time on the order of 10 s. The calculated permeabilities of the ABA and the AqpZ-ABA vesicles were 0.8 μm/s and 74 μm/s, respectively. This indicates that protein incorporation leads to a large permeability increase—almost 90 times greater than the polymer vesicles. Assuming the polymer vesicles have the molecular weight estimated from the light-scattering experiments, a maximum of 25 monomers per vesicle is possible. Then, using the calculated permeability of 74 μm/s and the estimated vesicle surface area based on radius measurements, the water permeability for each AqpZ tetramer is calculated as 13×10^{-14} cm^3/s,
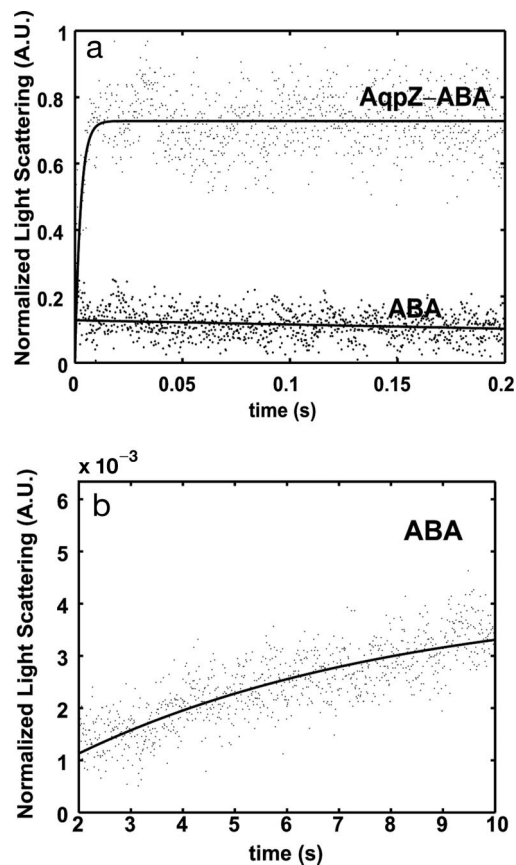
Fig. 2. Stopped-flow light-scattering experiments. (*a*) Increase in relative light scattering with and without reconstituted AqpZ into the ABA polymer at 5.5°C at a molar ratio of 200:1 (polymer:protein). Fits are shown as guides. The initial rise rates were used to calculate the permeability. As seen from *a*, a rise cannot be calculated for the pure ABA polymer vesicles. (*b*) Shown is the rise in scattering between 2 and 10 s for the ABA vesicles that was used in calculating permeability at 5.5°C.

which is similar to values reported for AqpZ reconstituted into liposomes [$\geq 10 \times 10^{-14}$ (5)].

Calculation of Activation Energies. Activation energies for water transport are calculated by conducting experiments over a wide range of temperatures, and these energies can be used to determine whether transport across vesicle membranes is diffusion-driven or channel-mediated. Calculated permeabilities for the AqpZ-ABA vesicles indicate an increase of 38 to 94 times over ABA vesicles in these experiments. In Fig. 3, the exponential constants obtained from these experiments are plotted against the inverse of temperature to determine the Arrhenius activation energies. The Arrhenius activation energy calculated for the ABA vesicles was 8.7 kcal/mol, whereas the AqpZ-ABA vesicles had a value of 3.4 kcal/mol. The higher value obtained for the ABA membrane is consistent with the values of activation energies reported for polymer membranes in the measured temperature range (30, 31), indicating transport by diffusion through the polymer. The low-activation energy for the AqpZ-ABA vesicles is strong evidence for channel-mediated water transport through AqpZ molecules. This value is also consistent with the low-activation energy values found in AqpZ-incorporated proteoliposomes (5) and AQP1-incorporated oocytes (3).

Reflection Coefficients. Solute reflection coefficient determines the extent to which a membrane excludes a particular solute. The
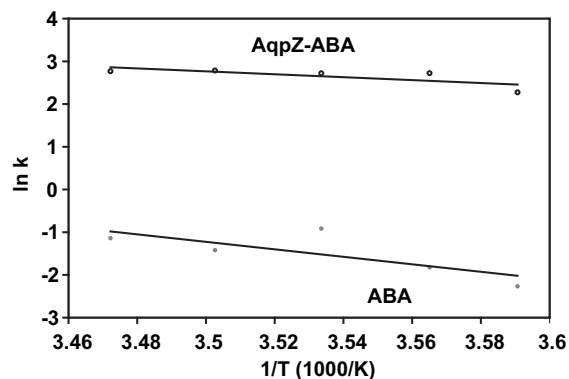

Fig. 3. Arrhenius plots for calculation of activation energy for osmotic transport of water across polymer membranes with incorporated AqpZ (AqpZ-ABA) and pure polymer membranes (ABA).

relative reflection coefficients of salt, urea, glucose, and glycerol were determined by using a procedure described by Meinild *et al.* (6). Glucose, with an assumed reflection coefficient of unity, was taken as the reference solute because of its relatively large molecular size. The calculated reflection coefficients of salt, glycerol, and urea were greater than one, indicating higher relative rejection of these solutes (data not shown). These reflection coefficients are higher than the values reported by Meinild *et al.* (6) for the same solutes, but agree within the experimental error for our calculations.

Effect of Protein-to-Polymer Ratio on Permeability. Stopped-flow experiments were conducted at 5.5°C with protein-to-polymer molar ratios of 1:25, 1:50 1:100, 1:200, 1:500, and 1:1000. Fig. 4 indicates a sharp permeability increase followed by a sharp decrease as the concentration of protein is increased. Permeability peaks at a protein-to-polymer ratio of 1:50 where the vesicle permeability is ≈3,000 times greater than the pure polymer.

Discussion

Large improvements in the efficiency of water treatment membranes may result from the development of biomimetic membranes with high permeability and selectivity. In this work, we describe the incorporation of the bacterial water-channel protein AqpZ into an ABA triblock copolymer and provide data on the permeability and selectivity of this new membrane. Permeability varied with the AqpZ:ABA ratio and showed an activation energy indicative of channel-mediated transport. Furthermore, the selectivity of the AqpZ-ABA membrane for water over small solutes such as salt, glucose, urea, and glycerol was demonstrated.

The orders-of-magnitude increase in permeability observed on incorporation of AqpZ indicates that the water-channel protein is functional in the synthetic context, as seen for other membrane proteins in a similar polymer (19). The magnitude of increase in permeability and the excellent solute rejection capabilities demonstrate the potential benefit of such membranes for water treatment and drug delivery. The ABA triblock copolymer was found to be relatively impermeable when compared with other membranes; its productivity was 0.22 $\mu m \cdot s^{-1} \cdot bar^{-1}$ at 20°C, which can be compared with the value of 5.7 $\mu m \cdot s^{-1} \cdot bar^{-1}$ at 20°C for a similar diblock copolymer [poly-ethylethylene–polyethylene oxide; calculated from Discher *et al.* (13)]. The large difference in the size and type of the hydrophobic blocks used here (110 units of dimethylsiloxane) and the diblock copolymer studied by Discher *et al.* (37 units of ethyleneethylene) could account for this difference. The permeabilities of lipid membranes are reported to be an order of magnitude
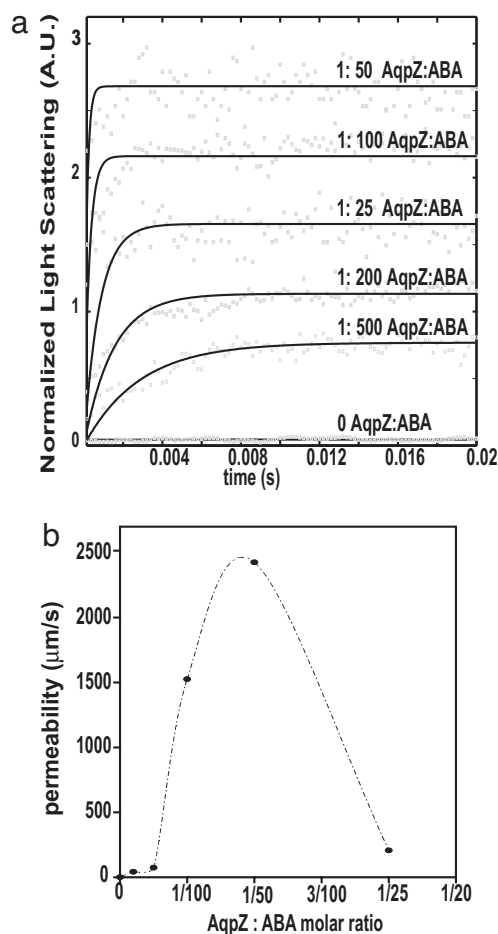
Fig. 4. Effect of increasing AqpZ concentrations on the permeability of ABA polymers. (*a*) Light-scattering results normalized to fit between 0 and 1. Curves for different ratios have been offset for clarity and fits are shown as guides. Data at 0 AqpZ:ABA ratio shown at a fixed offset. (*b*) Increase in calculated permeability with increase in protein-to-polymer molar ratio.

Fig. 5. Comparison of reported permeability values for polymeric membranes to those obtained in this study. FO is a commercial forward-osmosis membrane with data from McCutcheon and Elimelech (37) at 20°C. RO is a commercial reverse-osmosis desalination membrane with data from Matsura (38) at room temperature (assumed 25°C). EE-EO is a polyethylethylene-polyethylene oxide diblock polymer with data from Discher *et al.* (13) at 20°C. ABA represents the polymer vesicles used in this study with permeability calculated at 20°C. AqpZ-ABA represents the polymer vesicles with incorporated AqpZ at 1:50 molar ratio used in this study at 20°C. Data for ABA and AqpZ were obtained at 5.5°C and calculated at 20°C by using E_a values.

higher than the polyethylethylene–polyethylene oxide copolymer (13). The incorporation of AqpZ increases the productivity of ABA membranes by ≈800 times (Fig. 5). Additionally, the productivities of AqpZ-ABA membranes reported here exceed those for any salt-rejecting membrane (Fig. 5). Although these values were measured by using different procedures, it can be seen from this comparison that the AqpZ-ABA protein-polymer system investigated here represents more than an order-of-magnitude improvement over existing reverse-osmosis and forward-osmosis membranes. Additional research will be needed to identify appropriate support materials and pretreatment that could lead to successful new water treatment schemes.

The AqpZ-ABA system studied here may benefit from further optimization of the protein incorporation conditions, leading hopefully to membranes with greater permeability. Increasing the amount of AqpZ leads first to a permeability increase, then to a permeability decrease—similar to the performance of lipid membranes. In experiments with lipid membranes, a limiting concentration of AqpZ was observed around a protein-to-polymer weight ratio of 1:200 (5). We see such a limiting concentration at a protein-to-polymer ratio of 1:19 (1:50 molar ratio). The difference may result from the fact that the molecular weight of the polymers used here is greater than lipid molecular weight. The limiting concentration observed is probably due to the method of incorporation used. Detergent concentration
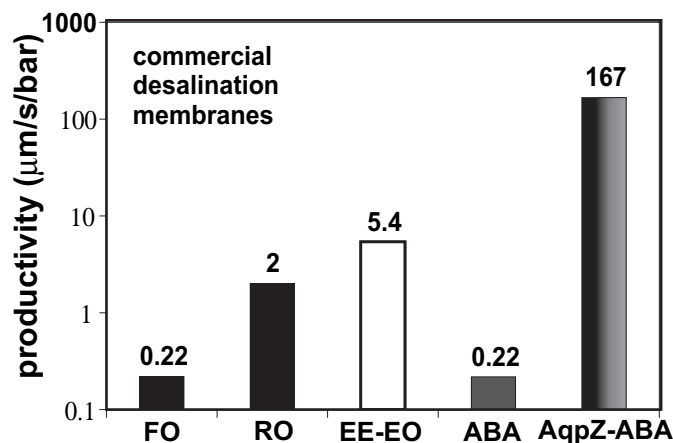
increases at the higher AqpZ concentrations because detergent is present in the AqpZ stock solution. This may have resulted in a low AqpZ reconstitution efficiency and lower permeabilities when higher volumes of AqpZ stock solution are used. Unfortunately, the number of AqpZs inserted per vesicle has not been determined in this or other AqpZ studies (5); hence, we cannot offer a definitive conclusion. However, other studies have shown that vesicles with a AqpZ-to-lipid weight ratio of 1:1 can be synthesized by using slow detergent removal methods (32, 33). This indicates that higher permeabilities might be possible with other reconstitution methods. These results also indicate that membranes with specified levels of water permeability can be synthesized by controlling the concentration of AqpZ—a property that may be useful for drug delivery applications.

The protein-polymer membranes developed here have salt rejection and permeability ideal for desalination. Excellent control over the permeability of polymers was also demonstrated. Incorporation of AQPs (or suitable molecular mimics) into compatible synthetic polymers (such as the block copolymer system investigated in this study) is an innovative approach for making membranes for medical, industrial, and municipal desalting applications.

Materials and Methods

The detergent dodecyl maltoside used in protein purification was obtained from Anatrace Chemicals. Ni-NTA agarose beads were obtained from Qiagen. Sepharose 4B was used for chromatographic separation and was obtained from Sigma Aldrich. Other chemicals were obtained as described in the following sections.

Expression and Purification of AQP-Z. The plasmid allowing overexpression of histidine-tagged AqpZ (pTrc10HisAqpZ) was obtained from Dr. Peter Agre (Duke University Medical Center, Durham, NC) (5). It was transformed into the *E. coli* strain JM109 by electroporation. The resulting strain was grown and protein production induced by addition of isopropyl-β-D-thiogalactoside according to Borgnia *et al.* (5) with two modifications. The induction time was optimized at 7–8 h. The ultracentrifugation setup for recovery of membrane fractions was replaced by the use of a Biomax filter (MWCO of 30 kDa) in a centrifuge for 45–60 min for removal of smaller-molecular-weight material. Protein purification was performed by using nickel affinity chromatography (5).

Protein purification was followed by solubilization with a standard SDS

cracking buffer (34) with an additional component, 1% dodecyl maltoside, and polyacrylamide gel electrophoresis (34) to determine presence of protein. The purified protein was quantified by using the Lowry method (35).

Synthesis of ABA Polymer. The ABA was a symmetric poly-(2-methyloxazoline)-block-poly-(dimethylsiloxane)-block-poly-(2-methyloxazoline) (PMOXA$_{15}$-PDMS$_{110}$-PMOXA$_{15}$) polymer. The first step of the synthesis procedure involved acid-catalyzed polycondensation of dimethoxydimethyl silane in the presence of water and end-capper, resulting in butylhydroxy-terminated bifunctional PDMS. Liquid PDMS was purified by vacuum stripping at 80°C and precipitation in an equal (by weight) water/methanol mixture. Purified PDMS was reacted with triflic acid anhydride in hexane at −10°C for 3 h, resulting in triflate-PDMS bifunctional macroinitiator. The reaction mixture was then filtered under argon through a G4 filter. Hexane was evaporated under vacuum and dry ethyl acetate was added as reaction solvent. Addition of dry 2-methyl-2-oxazoline resulted in symmetric ring-opening cationic polymerization of PMOXA blocks on the macroinitiator. The reaction was terminated by addition of a methanol solution of 0.5 M potassium hydroxide. The synthesis of a similar, lower-molecular-weight polymer system with a lower hydrophobic-to-hydrophilic block-length ratio is described in further detail in Nardin *et al.* (26).

Preparation of ABA Vesicles and AQP Incorporation. Block copolymer vesicles (1–2 wt % of polymer in PBS at pH 7.4) were prepared by using the film rehydration method. Sixty milligrams of polymer was first dissolved in chloroform (5–10 ml), and the chloroform was evaporated slowly in a rotary vacuum evaporator at 40°C and a vacuum of <400 mbar to form an even film on the inside of round-bottomed flasks. This film was then further dried under a 0.3-mbar high vacuum for at least 4 h. Ten milliliters of PBS was then added dropwise to the film with alternating vigorous vortexing and periodic sonication (of durations <30 s) for several minutes. This mixture was then left stirring for at least 8 h. The resulting suspension was extruded several times through a 0.4-μm track-etched filter (Isopore, Millipore), followed by a 0.2-μm track-etched filter (Nucleopore, Whatman) to obtain monodispersed unilamellar vesicles. For reconstitution experiments, 500 μl of an AqpZ stock solution (1.6 mg/ml in 1.5% dodecyl maltoside, 66 mM KH$_2$PO$_4$, 133 mM NaCl, 13% glycerol, 3.33 mM β-mercaptoethanol, and 33.33 mM Tris) was added during the formation of the polymer vesicles, and subsequent steps were completed on ice. The resulting protein-containing vesicles were purified chromatographically by using a column packed with Sepharose 4B to remove nonincorporated protein and trace detergent.

Characterization of Vesicles. *Light scattering*. The static and dynamic light-scattering experiments were performed according to Nardin *et al.* (26) by using a commercial goniometer (ALV) equipped with a He-Ne laser (wavelength, 633 nm) at scattering angles between 30° and 150°. An ALV-5000/E correlator was used to calculate the photon intensity, and an autocorrelation function was used to calculate vesicle size.

Atomic force microscopy. These measurements were conducted by using a Picoscan SPM LE scanning-probe microscope equipped with a Picoscan 2100 SPM controller (Agilent Technologies). Measurements were conducted in tapping mode by using a Si cantilever (NCH) (Nanosensors). The length of this cantilever was 125 μm and the nominal force constant was 42 N/m. Samples were prepared by placing a dilute vesicle suspension on freshly cleaved mica for 1 min and then carefully washing with double-distilled water. This sample was dried and the measurements were performed on dry samples.

Transmission electron microscopy. These measurements were conducted on vesicle samples by using a Philips 400 microscope (Philips). The samples were prepared by dilution up to 1,000 times and then stained with 2% uranyl acetate on plasma-treated copper grids.

Cryogenic transmission electron microscopy. The vesicle suspension was deposited on a holey carbon grid and frozen rapidly by plunging into liquid ethane above its freezing point by using a cryo holder. This holder was then transferred to the microscope and imaged in transmission mode at 200 kV at liquid nitrogen temperature. The equipment used for this measurement was a Zeiss 922 Omega microscope with a Gatan CT3500 cryo holder and a Gatan Ultrascan 1000 camera system.

Permeability measurements. The permeability of the two types of vesicles were determined by using a stopped-flow procedure (5). The stopped-flow apparatus was a SX.17 MV spectrometer (Applied Photophysics). Vesicles were rapidly mixed with a solution containing the osmotic agent (salt, glucose, glycerol, or urea) causing water efflux from the vesicles. The changes in light scattering caused by vesicle shrinkage were recorded at an emission wavelength of 600 nm in the stopped-flow apparatus [Borgnia *et al.* (5) and Milon *et al.* (36)]. These experiments were conducted with a constant 7-bar pressure to minimize pressure variations that could complicate kinetics analysis. Results were corrected for pressure-related mechanical compression by subtracting the baseline observed in control experiments without osmotic agents. These data were then fitted to an exponential rise equation to calculate the exponential coefficient, and the osmotic water permeability (P_f) was calculated by using the following expression (5):

$$P_f = k/(S/V_o) \times V_W \times \Delta_{osm},$$

where k is the exponential rise rate constant for the initial rise in the light-scattering curve, S is the initial surface area of the vesicles, V_o is the initial volume of the vesicles, V_W is the molar volume of water (18 cm^3), and Δ_{osm} is the difference in osmolarity driving the shrinkage of the vesicles.

Several sets of experiments were conducted with similar conditions but different preparations (prepared in different batches) to ensure repeatability. Additionally, initial experiments with up to 12 traces per experimental condition showed that five traces were adequate for providing sufficient data for analysis. Therefore, in subsequent analyses, a minimum of five traces were fit to the initial exponential rise by using the curve-fitting toolbox available through the MATLAB software (Mathworks).

Stopped-flow experiments were repeated at different temperatures (5.5, 7.5, 10, 12.5, and 15°C) for the ABA and AqpZ-ABA vesicles. The exponential rise rates calculated from these experiments were plotted against the inverse of temperature to determine the Arrhenius activation energies.

The reflection coefficients for salt, urea and glycerol were calculated based on the method presented by Meinild *et al.* (6). Glucose was used as the reference solute and the comparative experiments were all conducted at 15°C.

1. Knepper MA, Wade JB, Terris J, Ecelbarger CA, Marples D, Mandon B, Chou CL, Kishore BK, Nielsen S (1996) *Kidney Int* 49:1712–1717.
2. Gorin MB, Yancey SB, Cline J, Revel J-P, Horwitz J (1984) *Cell* 39:49–59.
3. Preston GM, Carroll TP, Guggino WB, Agre P (1992) *Science* 256:385–387.
4. Nielsen S, Smith BL, Christensen EI, Agre P (1993) *Proc Natl Acad Sci USA* 90:7275–7279.
5. Borgnia MJ, Kozono D, Calamita G, Maloney PC, Agre P (1999) *J Mol Biol* 291:1169–1179.
6. Meinild AK, Klaerke DA, Zeuthen T (1998) *J Biol Chem* 273:32446–32451.
7. Jung JS, Preston GM, Smith BL, Guggino WB, Agre P (1994) *J Biol Chem* 269:14648–14654.
8. Pontoriero G, Pozzoni P, Andrulli S, Locatelli F (2003) *Nephrol Dial Transplant* 18(Suppl 7):vii21–vii25.
9. Pastan S, Bailey J (1998) *N Engl J Med* 338:1428–1437.
10. Service RF (2006) *Science* 313:1088–1090.
11. Tal A (2006) *Science* 313:1081–1084.
12. Patel-Predd P (2006) *Environ Sci Technol* 40:3454–3455.
13. Discher BM, Won YY, Ege DS, Lee JCM, Bates FS, Discher DE, Hammer DA (1999) *Science* 284:1143–1146.
14. Dinsmore AD, Hsu MF, Nikolaides MG, Marquez M, Bausch AR, Weitz DA (2002) *Science* 298:1006–1009.
15. Coury LA, Mathai JC, Brodsky JL, Agre P, Zeidel ML (1996) *J Am Soc Nephrol* 7:A0088–A0088.
16. Duncan R (2003) *Nat Rev Drug Discov* 2:347–360.
17. Taubert A, Napoli A, Meier W (2004) *Curr Opin Chem Biol* 8:598–603.
18. Meier W, Nardin C, Winterhalter M (2000) *Angew Chem Int Ed* 39:4599–4602.
19. Graff A, Sauer M, Van Gelder P, Meier W (2002) *Proc Natl Acad Sci USA* 99:5064–5068.
20. Choi HJ, Montemagno CD (2005) *Nano Lett* 5:2538–2542.
21. Choi HJ, Germain J, Montemagno CD (2006) *Nanotechnology* 17:1825–1830.
22. Stoenescu R, Graff A, Meier W (2004) *Macromol Biosci* 4:930–935.

23. Leson A, Filiz V, Forster S, Mayer C (2007) *Chem Phys Lett* 444:268–272.
24. Nardin C, Winterhalter M, Meier W (2000) *Langmuir* 16:7708–7712.
25. Nardin C, Thoeni S, Widmer J, Winterhalter M, Meier W (2000) *Chem Commun* 1433–1434.
26. Nardin C, Hirt T, Leukel J, Meier W (2000) *Langmuir* 16:1035–1041.
27. Grumelard J, Taubert A, Meier W (2004) *Chem Commun* 1462–1463.
28. Sulkowski E (1985) *Trends Biotechnol* 3:1–7.
29. Almgren M, Edwards K, Karlsson G (2000) *Colloids Surfaces A* 174:3–21.
30. Garybobo CM (1971) *J Gen Physiol* 57:610–622.
31. Mehdizadeh H, Dickson JM, Eriksson PK (1989) *Ind Eng Chem Res* 28:814–824.
32. Scheuring S, Ringler P, Borgnia M, Stahlberg H, Muller DJ, Agre P, Engel A (1999) *EMBO J* 18:4981–4987.
33. Dolder M, Engel A, Zulauf M (1996) *FEBS Lett* 382:203–208.
34. Sambrook J, Fritsch EF, Maniatis T (1989) *Molecular Cloning: A Laboratory Manual* (Cold Spring Harbor Lab Press, Cold Spring Harbor, NY).
35. Lowry OH, Rosebrough NJ, Farr AL, Randall RJ (1951) *J Biol Chem* 193:265–275.
36. Milon A, Lazrak T, Albrecht AM, Wolff G, Weill G, Ourisson G, Nakatani Y (1986) *Biochim Biophys Acta* 859:1–9.
37. McCutcheon J, Elimelech M (2006) *J Membr Sci* 284:237–247.
38. Matsura T (2001) *Desalination* 134:47–54.